

This is the revision of 2023, 16th February, of author's copy of the accepted publication as archived with the DLR's electronic library at <http://elib.dlr.de>. Please consult the original publication for citation, see e.g. <https://www.doi.org/10.1109/VPPC55846.2022.10003375>

# IEEE VTS Motor Vehicles Challenge 2023: A Multi-physical Benchmark Problem for Next Generation Energy Management Algorithms

J. Brembeck, R. de Castro, J. Tobolar, and I. Ebrahimi

This article presents a benchmark problem that researchers can use to evaluate the performance of energy management algorithms for multi-energy source and multimotor electric vehicles. The model makes use of Modelica, an open source, a-causal, object-oriented language for modeling cyber-physical systems in multi-domains (e.g. electrical, mechanical, thermal) of the vehicle components. The model also includes the aspect of three-dimensional mechanics, which enables completely new degrees of freedom in the controller design in comparison to one-dimensional approaches. To support interoperability among multiple design tools, the Modelica vehicle model is provided as a Functional Mockup Unit, an industry standard for exchange of simulation models. A set of standardized input-output interfaces and key performance metrics is also provided in the benchmarking problem, enabling the systematic ranking of multiple energy management strategies.

## Copyright Notice

©2022 IEEE. Personal use of this material is permitted. Permission from IEEE must be obtained for all other uses, in any current or future media, including reprinting/republishing this material for advertising or promotional purposes, creating new collective works, for resale or redistribution to servers or lists, or reuse of any copyrighted component of this work in other works.

J. Brembeck, R. de Castro, J. Tobolar, and I. Ebrahimi, "IEEE VTS Motor Vehicles Challenge 2023: A Multi-physical Benchmark Problem for Next Generation Energy Management Algorithms", 2022 IEEE Vehicle Power and Propulsion Conference (VPPC), Merced, California, USA, 2022.

# IEEE VTS Motor Vehicles Challenge 2023: A Multi-physical Benchmark Problem for Next Generation Energy Management Algorithms Updated Metrics

Jonathan Brembeck  
Institute of System Dynamics  
and Control (SR)  
German Aerospace Center (DLR)  
Oberpfaffenhofen, Germany  
[jonathan.brembeck@dlr.de](mailto:jonathan.brembeck@dlr.de)  
ORCID: 0000-0002-7671-5251

Ricardo de Castro  
Dept. of Mechanical  
Engineering  
University of California  
Merced  
[rpintodecastro@ucmerced.edu](mailto:rpintodecastro@ucmerced.edu)  
ORCID: 0000-0002-5546-3999

Jakub Tobolář  
Institute of System Dynamics  
and Control (SR)  
German Aerospace Center (DLR)  
Oberpfaffenhofen, Germany  
[jakub.tobolar@dlr.de](mailto:jakub.tobolar@dlr.de)  
ORCID: 0000-0002-4888-4664

Iman Ebrahimi  
Dept. of Mechanical  
Engineering  
University of California  
Merced  
[iebrahimi@ucmerced.edu](mailto:iebrahimi@ucmerced.edu)  
ORCID: 0000-0003-0130-8712

**Abstract**—This article presents a benchmark problem that researchers can use to evaluate the performance of energy management algorithms for multi-energy source and multi-motor electric vehicles. The model makes use of Modelica, an open source, a-causal, object-oriented language for modeling cyber-physical systems in multi-domains (e.g. electrical, mechanical, thermal) of the vehicle components. The model also includes the aspect of three-dimensional mechanics, which enables completely new degrees of freedom in the controller design in comparison to one-dimensional approaches. To support interoperability among multiple design tools, the Modelica vehicle model is provided as a Functional Mockup Unit, an industry standard for exchange of simulation models. A set of standardized input-output interfaces and key performance metrics is also provided in the benchmarking problem, enabling the systematic ranking of multiple energy management strategies.

**Keywords**—energy management, vehicle dynamics control, electro-mobility, trajectory control, battery model, Modelica, Functional Mockup Interface, hydrogen fuel cell, multi-physical modelling, drivetrain models

## I. INTRODUCTION

In order to stimulate advances in vehicular energy and power management, the IEEE Vehicular Technology Society (VTS) initiated the VTS Motor Vehicles Challenge in 2016. The competition’s themes have focused on energy management of hybrid energy storage systems (fuel cells/batteries/supercapacitors [1] [2] [3] [4]) and their applications to cars ([5] [6]), trucks [7] and trains [8]. These competitions provide benchmark problems where researchers can evaluate and compare the performance of their energy management algorithms against other research groups.

In this year’s competition we bring a new dimension to the challenge: torque allocation in multi-motor electric vehicles. In addition to managing a hybrid energy storage system, the competitors are asked to develop torque allocation for a four-wheeled vehicle with three traction motors: two (rear) in-wheel motors and one front motor. This multi-motor configuration offers various advantages. It can enhance energy efficiency of the vehicle by enabling energy recuperation in both front and rear axle [9] and also decreasing tire slip losses [10]. It improves motion control of the vehicle by extending the maximum lateral acceleration [11] and decreases response of inner (yaw-rate) control loops. This last feature is particularly attractive to improve tracking performance and vehicle dynamics stability of path/trajectory following algorithms of autonomous vehicles [12]. It also offers redundant traction actuators that can be exploited by fault tolerant controllers to improve vehicle reliability [13].

As reference vehicle for this year’s competition we employed an adapted version of the DLR ROboMObil ([14] [15] [16] [17]), which is extended here with a hydrogen fuel cell. To model this vehicle, we make use of Modelica [18], an open source, a-causal, object-oriented language that allows the modeling of cyber-physical systems in multi-domains, e.g. electrical, thermal and mechanical. It also offers powerful model inversion capabilities, which facilitate the design of non-linear motion control algorithms [19].

Since there is a manifold of simulators on the market, we decided to export the vehicle model through the functional mockup interface (FMI) [18] technology. This allows the competitors to develop a control strategy using their tool of choice. Our simulation model gives the benefit of a very high computational efficiency, with an average real-time factor larger than twenty on a standard PC, which can be particularly useful to accelerate the development of learning-based control algorithms (e.g. [20]).

The paper is arranged as follows: Section II gives a general overview of the challenge; Section III introduces the Modelica model of the ROboMObil; Section IV describes the evaluation process and ranking of energy management algorithms. Section V summarizes all development steps and provides a look into future research.

## II. OVERVIEW OF THE CHALLENGE

As depicted in Figure 1, the challenge considers the ROboMObil vehicle with a hybrid energy storage system (fuel cell & hydrogen tank and battery), two in-wheel electric motors installed in the rear axle ( $\tau_{RL}$ ,  $\tau_{RR}$ ), one central front motor ( $\tau_F$ ), and a front steer-by-wire actuation ( $\delta$ ). These actuators are manipulated by the vehicle's motion controller in order to track a pre-defined reference velocity ( $v^*$ ) and track curvature ( $\rho^*$ ).

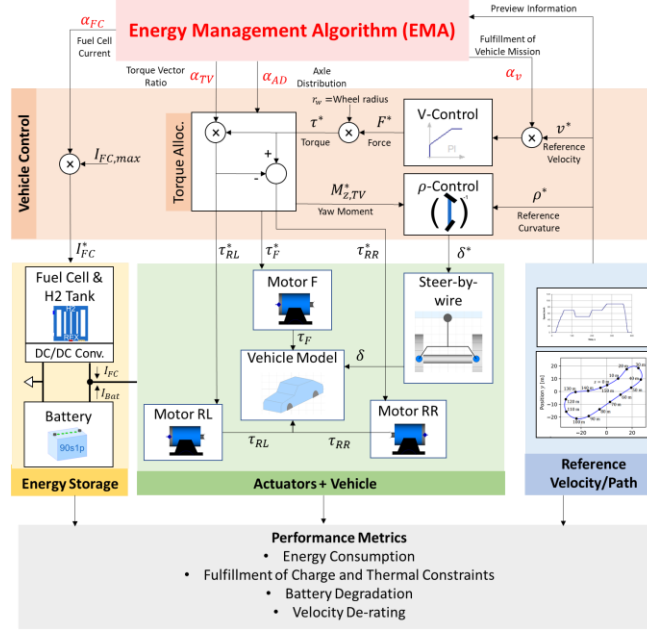


Figure 1: Block diagram of the benchmark problem.

The competitors are invited to develop the energy management algorithm (EMA) for the vehicle (Figure 1 – top red block). The EMA determines the operating conditions for the two energy storage devices and the three electric motors; minimization of the energy consumption and battery degradation are some of the main goals of the EMA.

### A. Energy Storage and Vehicle Actuators

The hybrid energy storage is composed of a 20 kW fuel cell and 20 kWh Li-ion battery. A DC/DC converter is connected to the fuel cell in order to regulate its current ( $I_{FC}$ ) and power flow between the hybrid storage elements. The hybridization with a hydrogen range extender (REX), being composed of the fuel cell and a hydrogen tank, enables the reduction of usage of rare elements like Lithium while enhancing the vehicle's range. Both the fuel cell & H2 tank and the battery provide energy to the two in-wheel motors and the central front motor. Because of their decoupled architecture, the in-wheel motors can generate non-symmetric torques in the left and right rear wheels and, thus induce additional yaw-moment to the vehicle's chassis. This yaw-moment can be exploited to enhance vehicle handling and safety [21]; it can also decrease the amount of front steering, thus reducing tire slip losses [10]. Additionally, a steer-by-wire actuator is installed in the front axle to modify the steering angle  $\delta$ .

### B. Mission Planning and Vehicle Control

We assume that the planning of the vehicle's mission is defined in advance, e.g. using trajectory planning methods such as [16]. The mission is characterized by a reference vehicle velocity  $v^*(t)$  and the track curvature  $\rho^*(t)$  over a given time horizon  $t \in [0, t_{end}]$ .

The motion controller tracks  $v^*$  through manipulation of the reference traction force  $F^*$ . This reference force is converted into a reference torque  $\tau^* = F^* r_w$ , with  $r_w$  being the wheel radius, which is then divided between the front and rear axle

$$\tau_F^* = \tau^* \alpha_{AD}, \quad \tau_R^* = \tau^* (1 - \alpha_{AD}), \quad (1)$$

where  $\alpha_{AD}$  indicates the variable front/rear axle distribution. Afterwards, the rear axle torque is allocated into left and right motor torques using a normalized torque vector ratio  $\alpha_{TV} \in [0, 1]$ :

$$\tau_{RR}^* = \tau_R^* \alpha_{TV}, \quad \tau_{RL}^* = \tau_R^* (1 - \alpha_{TV}). \quad (2)$$

When  $\alpha_{TV} = 0.5$ , both motors receive the same torque;  $\alpha_{TV} = 1$  allocates all the torque solely to the right motor and  $\alpha_{TV} = 0$  solely to the left motor. Additionally, all electric motors are subject to torque constraints:

$$\tau_{min,i} \leq \tau_i^* \leq \tau_{max,i}, \quad (3)$$

where  $i \in \{F, RR, RL\}$  is the motor index,  $\tau_{min,i}$  the minimum allowed torque and  $\tau_{max,i}$  the maximum allowed torque.

The reference curvature  $\rho^*$  is tracked through the manipulation of the steering angle  $\delta^*$ , while considering the additional yaw-moment generated by the torque vectoring. Note that, throughout this document, the superscript  $x^*$  is used to denote the desired value for the variable  $x$ .

### C. Energy Management Algorithm (EMA)

The EMA is responsible for computing four control variables, cf. the red variables in Figure 1 top:

1. the normalized fuel cell current,  $\alpha_{FC} \in [0,1]$ , which affects the power split between the battery and the fuel cell (note  $I_{FC}^* = \alpha_{FC} I_{FC,max}$ , where  $I_{FC,max}$  is the maximum allowed fuel cell current);
2. the axle torque distribution ratio,  $\alpha_{AD} \in [0,1]$ , to determine the front and rear distribution of the desired torque  $\tau^*$ , see eq. (1).
3. the torque vectoring ratio,  $\alpha_{TV} \in [0,1]$ , to determine the torque allocation between right and left motors, see eq. (2).
4. the velocity derating factor,  $\alpha_v \in [0,1]$ , which decreases the reference velocity  $v^*$  to  $\alpha_v v^*$  (see Figure 1); it offers an additional degree of freedom to prevent violation of safety constraints in the system (e.g. over-discharge of the battery).

The EMA provided by the competitors will be evaluated using a wide range of performance metrics, including energy consumption, violation of safety constraints, battery degradation and fulfillment of the vehicle’s mission (also referred as velocity derating in the sequel). These metrics will be defined in more detail in Section IV.

The EMA will have access to several states of the vehicle and energy storage, such as battery state of charge, temperature, etc. Additionally, it will also receive a short preview of future values of the velocity and curvature references:

$$\hat{v}(t + \Delta t), \hat{\rho}(t + \Delta t), \quad (4)$$

where  $\Delta t \in [0, \Delta t_{max}]$  and  $\Delta t_{max}$  is the preview window which is available in map data systems with a virtual horizon. This preview information can be generated by the trajectory planning module of the vehicle.

## III. COMPONENTS MODELING

In this section we briefly describe the Modelica model of the ROboMObil ([16], [17]) vehicle with a slightly modified architecture for this challenge, depicted in Figure 1. The aim is to describe the most relevant physical laws and effects with the focus on a numerical efficient simulation, which is necessary for a quick assessment of the EMAs or a machine learning process to synthesize the controller.

### A. ROboMObil’s Chassis Model

To capture the fundamental dynamics of the ROboMObil, we use a double track model implemented with the Modelica planar mechanics library [22]. It offers three degrees of freedom: the vehicle can move in longitudinal and lateral direction and rotate about the vertical axis. The chassis model, depicted in Figure 2, consists of a front and rear axle, both with wheels, a car body and air resistance.

In addition, the model contains three types of interfaces: mechanical (gray and white circles), thermal (red squares) and control (yellow connectors). The mechanical interfaces are used to exchange position and torque/force of mechanical elements. The heat interface captures the heat flow between components, and allows to quantify the energy losses that are eventually dissipated to the environment. The control interfaces contain signals that are generated by sensors (e.g. acceleration signal recorded by an inertial measurement unit) and control modules (e.g., steering actuator demand).

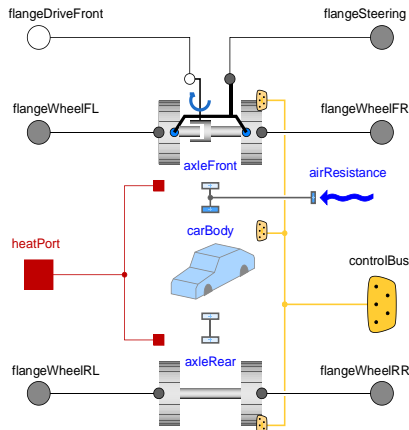


Figure 2: Structure of the Modelica planar vehicle model

The rigid front axle is assembled from an open differential that distributes the torque of the central front motor – provided by “flangeDriveFront” connector in Figure 2 – to the left and right wheel, which utilizes a slip-based tire model, see Section III.B. Moreover, a steering mechanism that equally transmits the steering input onto both left and right front wheels is implemented.

The rigid rear axle is, in contrast, composed only of two slip-based tire models. They can be directly driven by torque sources connected from outside to connectors “flangeWheelRL” and “flangeWheelRR” for left and right wheel, respectively. In this way, an in-wheel drive can be realized.

### B. Slip-based Tire Model with Losses

ROboMObil’s four wheels are modelled with a slip-based tire model [23] which is extended with energy loss effects. To simplify the model, tire load fluctuation during cornering or braking/accelerating are neglected and the wheel is bounded to the track-plane (holonomic-constraint). While operating at constant load  $f_N$ , the slip velocity  $v_{slip}$  at the contact patch determines the slip forces according to Coulombs’s law for dry-friction characteristics,

$$f_i = -f_N \mu(v_{slip}) \frac{v_{slip,i}}{v_{slip}}. \quad (5)$$

Eq. (5) can be used for both the longitudinal ( $i = long$ ) and the lateral ( $i = lat$ ) direction, resolved in the wheel coordinate system. The friction coefficient  $\mu$  depends on the slip velocity  $v_{slip}$ . To construct this dependency, we follow the approach developed in [23] and utilize two pairs of parameters: ( $v_{adhesion}$ ,  $\mu_A$ ) and ( $v_{slide}$ ,  $\mu_S$ ). The former pair determines maximum friction  $\mu_A$  at  $v_{slip} = v_{adhesion}$ . The latter pair specifies a sliding area by friction  $\mu_S$  at slip velocities  $v_{slip} \geq v_{slide}$ .

The rolling motion of the wheel can be actuated by the driving or braking torque input, cf. “flangeWheelXY” in Figure 2, with X denoting front (“F”) of rear (“R”) position of the wheel and Y denoting its left (“L”) or right (“R”) side.

The tire losses comprise losses at tire/road contact area due to the dry-friction contact and are expressed with the power loss

$$P_{loss} = v_{slip} \sqrt{f_{long}^2 + f_{lat}^2}. \quad (6)$$

### C. Battery Model with Aging Degradation

To obtain a good tradeoff between simulation speed and modeling accuracy, we modeled the battery with an equivalent electrical circuit model. This circuit consists of an ideal voltage source ( $U_{OCV}$ ) in series with an internal resistance ( $R_i$ ). The terminal voltage of the cell is described as

$$u_{cell} = U_{OCV}(SoC_b) - R_i(SoC_b) \cdot i_{cell}, \quad (7)$$

where  $i_{cell}$  is the current in the battery cell.

Both the internal voltage and resistance depend on the battery state of charge ( $SoC_b$ ), a normalized indicator for the amount of charge stored in the battery. Lookup tables are employed to characterize this variation, but are limited to room temperature values. A more complex implementation with temperature dependency is given in [24].

In Figure 3 the functional model of the battery pack is shown. On the left side we have the electrical connectors (in blue), which propagate the electric signals (voltage and current) to the other components in the vehicle, while on the right side we have the  $SoC_b$  calculation realized by an integrator ( $calc\_SoC_b$ ), in dependency of the nominal cell capacity  $C_{cell,0}$ . The pack is scaled by the number of in serial  $no_s$  and in parallel  $no_p$  connected cells. The battery model also contains a simple thermal model that captures heat flow between the battery cell and a (constant-temperature) environment using a thermal resistor.

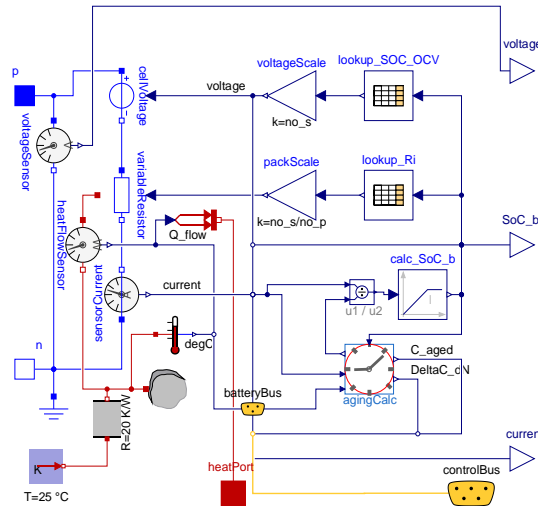


Figure 3: The equivalent circuit battery model in Modelica

The battery model also includes an aging model ( $agingCalc$  in Figure 3) for predicting the capacity degradation of the battery due to the charge/discharge events. This aging is computed using the average current ( $i_{avg}$ ) and temperature ( $T_{avg}$ ) of the

battery over a discharge cycle, as described in [25] p. 1232. The normalized cell capacity loss during the drive cycle  $\Delta C_{cell}$  is calculated as

$$\begin{aligned} \Delta C_{cell}(i_{avg}, T_{avg}, N) &= \\ &= \underbrace{\theta_1 \exp\left(-\frac{\theta_4}{T_{avg}} + \left(\theta_2 + \frac{\theta_5}{T_{avg}} i_{avg}\right)\right)}_{\text{start of battery lifetime - slow aging}} N^{\theta_3} \\ &+ \underbrace{\theta_8 \exp(N - N_{knee} \theta_7)}_{\text{"late" battery lifetime - fast aging}}, \end{aligned} \quad (8)$$

where  $\theta_i$  are aging parameters taken from experiments carried out in [25]. The parameter  $N$  is the number of discharge cycles and  $N_{knee} = \theta_6 + \theta_9 \cdot i_{avg} + \theta_{10} \cdot T_{avg}$  is a parameter point where the battery aging accelerates. The remaining cell capacity, in dependency of the initial cell capacity  $C_{cell,0}$  is defined as

$$C_{aged} = (1 - \Delta C_{cell})C_{cell,0}. \quad (9)$$

To facilitate the evaluation of the EMA, we focus on the rate of aging of the battery during the driving cycle. It is determined via a linearization of  $\Delta C_{cell}$  around the current number of cycles  $\bar{N}$  as follows

$$\begin{aligned} \frac{d\Delta C_{cell}(i_{avg}, T_{avg})}{dN} &= \left. \frac{d\Delta C_{cell}(i_{avg}, T_{avg}, N)}{dN} \right|_{N=\bar{N}} \\ &= \theta_1 \exp\left(-\frac{\theta_4}{T_{avg}} + \left(\theta_2 + \frac{\theta_5}{T_{avg}} i_{avg}\right)\right) \theta_3 \bar{N}^{\theta_3-1}. \end{aligned} \quad (10)$$

#### D. Quasi-Stationary Electric Motor Model

The three traction motors installed in the vehicle (cf. Figure 1) rely on permanent magnet synchronous machines (PMSM). They are represented using a quasi-stationary model (Figure 4) with the variables listed in Table 1. The fundamental electric machine equations  $d\Psi_d/dt$  and  $d\Psi_q/dt$  of the stator flux are given as:

$$\frac{d\Psi_d}{dt} = U_d - R_s I_d + \Omega_L \underbrace{L_1 I_q}_{\Psi_q}, \quad (11)$$

$$\frac{d\Psi_q}{dt} = U_q - R_s I_q - \Omega_L \underbrace{(\Psi_{PM} + L_1 \cdot I_d)}_{\Psi_d}. \quad (12)$$

These equations are easily implemented in Modelica using the acausal equation environment, i.e. all equation hold for the four quadrants of operation of the electric machine and are not dependent on any signal flow direction [26].

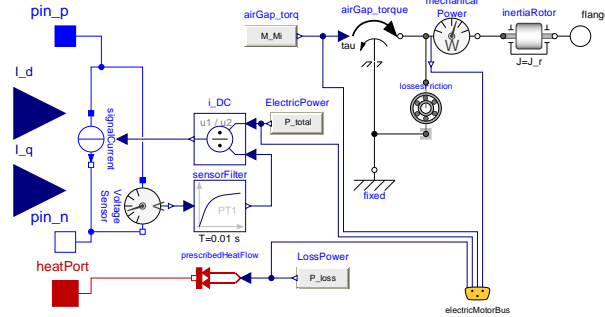


Figure 4: Quasi-stationary PMSM model

To prevent a slow simulation, the electric motor model and its controller are designed in the rotating d/q-frame and the reverse transformation to the a/b/c phases is not explicitly implemented. The closed-loop response of the motor current ( $I_q$ ) controller is approximated by a second-order transfer function with cut-off frequency 100 Hz.

Table 1: PMSM variables description

| Quantity  | Unit     | Description               |
|-----------|----------|---------------------------|
| $U_{d/q}$ | V        | Voltage in d-/q-axis      |
| $I_{d/q}$ | A        | Current in d-/q-axis      |
| $L_1$     | H        | Inductance in d- & q-axis |
| $R_s$     | $\Omega$ | Warm resistance per phase |
| $p$       | -        | Pole pair number          |

|              |       |   |
|--------------|-------|---|
| $\psi_{PM}$  | Wb    | Magnetic flux of permanent magnets            |
| $\psi_{d/q}$ | Wb    | d-/q- component of stator flux                |
| $\omega_L$   | rad/s | (Normed) Electrical angular velocity of rotor |

The model of the electric machine neglects reluctance influences ( $L_d = L_q = L_1$ ). Its air-gap torque is calculated as follows:

$$\tau_{jk} = M_{Mi} = 3/2 \cdot p \cdot \Psi_{PM} \cdot I_q. \quad (13)$$

Besides this quasi-stationary electric machine model, we also consider the energy losses within the PMSM, summed up in  $P_{loss} = P_{loss,inv} + P_{cop} + P_{iron} + P_{fric}$  in Figure 4:

Inverter losses (switching and basic load)

$$P_{loss,inv} = P_{inv,const} + k_{inv} \cdot I_q. \quad (14)$$

Copper losses (coil resistance)

$$P_{cop} = (\sqrt{3/2} \cdot I_q)^2 \cdot R_s. \quad (15)$$

Iron losses (also known as core losses)

$$P_{iron} = k_{hyst} \cdot \omega_m + k_{eddy} \cdot \omega_m^2. \quad (16)$$

Mechanical losses (friction effects, e.g., in bearings)

$$P_{fric} = k_{fric} \cdot \omega_m. \quad (17)$$

### E. Hydrogen Fuel Cell Model – Update Beta 2

The fuel cell model relies on a quasi-stationary model as proposed in [27] and depicted in Figure 5.

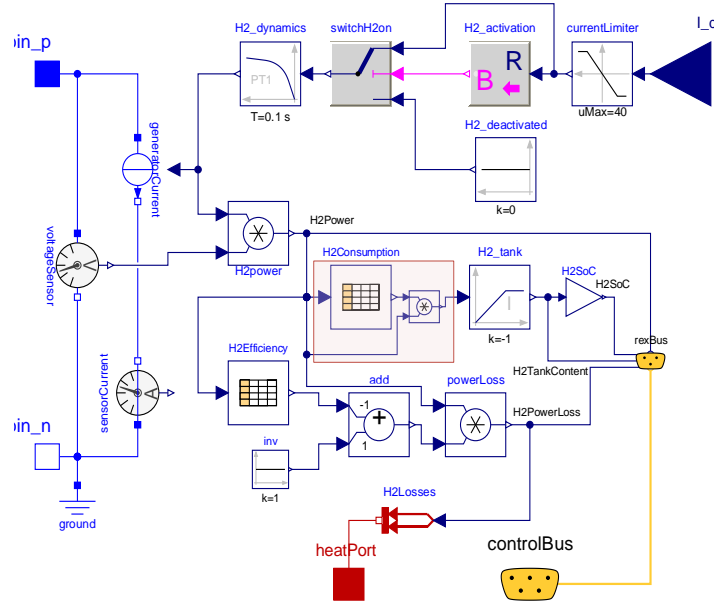


Figure 5: Functional hydrogen range extender model – Beta 2 Update modified part highlighted in red

Whenever a demanded current  $I_{dem}$  exceeds a minimum threshold (1 A in our model), the functional model approximates the fuel cell's output current using first order system dynamics. The fuel consumption relies on two tables. The first table maps the necessary hydrogen mass flow that is taken from the tank (Figure 6 – blue line), modelled as an integrator, whereas the second table maps the efficiency (Figure 6 – green line) depending on the point of operation.

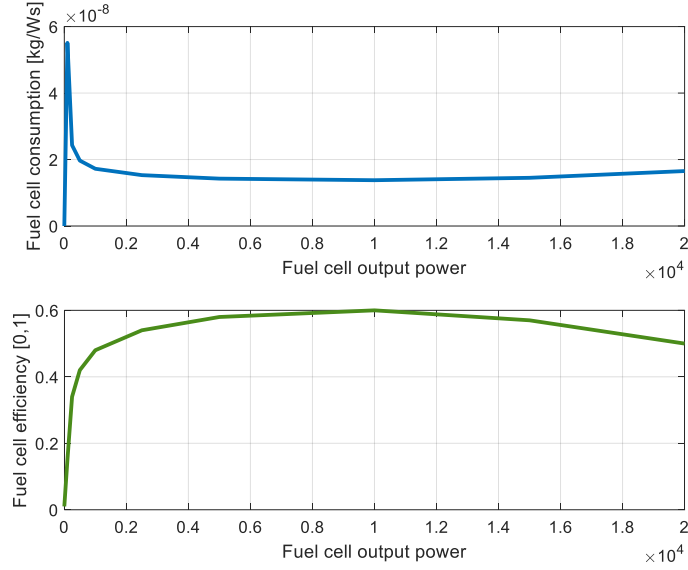


Figure 6: Revised for Beta 2 - Efficiency and hydrogen consumption map of the fuel cell based on [27]

#### F. Vehicle Motion Controller

The longitudinal velocity control relies on a linear PI controller [28]. The lateral controller uses a model inversion technique to follow the reference curvature ( $\rho^*$ ) generated by the mission planner. It makes use of a simplified single-track model [29]

$$\begin{aligned} \dot{x}_{STM} &= A(v^*)x_{STM} + B(v^*)\delta^* + E(v^*)M_{z,TV} \\ \beta^* &= v^*\rho^* - r^*, \end{aligned} \quad (18)$$

where  $x_{STM} = [\beta^*, r^*]^T$  is vector with the reference side-slip angle and yaw rate;  $A(v^*)$  and  $E(v^*)$  are matrices that depend on the vehicle velocity;  $M_{z,TV}$  is the torque vectoring generated by the in-wheel motors:

$$M_{z,TV} \approx \frac{c}{2r_w}(\tau_R^* - \tau_L^*) = \frac{c\tau^*}{2r_w}(2\alpha_{TV} - 1), \quad (19)$$

where  $r_w$  is the wheel radius and  $c$  the vehicle's track width. Assuming slow variations in vehicle curvature we can obtain

$$\begin{aligned} 0 &\approx A(v^*)x_{STM} + B(v^*)\delta^* + E(v^*)M_{z,TV} \\ 0 &\approx v^*\rho^* - [0, 1]x_{STM}, \end{aligned} \quad (20)$$

which represents a system of three linear equations with three unknowns  $(\delta^*, x_{STM}) = (\delta^*, \beta^*, r^*)$ . The steering angle applied to the vehicle is computed from the solution of these equations:

$$\delta^* = f_\delta(v^*, M_{z,TV}, \rho^*). \quad (21)$$

This represents a feedforward control law, which allows the vehicle to follow the reference curvature ( $\rho^*$ ) when the model uncertainty is reduced.

#### IV. ENERGY MANAGEMENT ALGORITHM

This section provides a brief overview of the requirements for the EMA that the competitors will need to develop, as well the scoring and ranking assessment of the competition.

##### A. Input/Output Interfaces

The EMA will have access to the following vehicle states

$$x = [v, a, SoC_b, T_b, SoC_{FC}, \widehat{W}] \in X_{EMA}, \quad (22)$$

which contain the current velocities  $v$ , accelerations  $a$ , state of charge  $SoC_b$  and temperature of the battery  $T_b$ , and the state of charge of the fuel cell  $SoC_{FC}$ . The variable  $\widehat{W}$  is a vector with a short preview information about the reference velocity and track curvature

$$\widehat{W} = \left( v^*(t + k\Delta t_p), \rho^*(t + k\Delta t_p) \right)_{k=0}^{N_{pre}}, \quad (23)$$

where  $\Delta t_p$  is the sample time and  $N_{pre}$  are the samples of the preview window. We denote  $X_{EMA}$  as the set of all possible combinations of states that the EMA might receive.

The EMA generates four output control signals, see Section II.C,

$$u = [\alpha_{FC}, \alpha_{AD}, \alpha_{TV}, \alpha_v] \in U = [0,1]^4, \quad (24)$$

where  $U$  represents the set of allowed control actions.

### B. Safety Constraints

The competitors will provide a control policy  $\pi$  for the energy management that maps the states into the control actions

$$\pi(x): X_{EMA} \rightarrow U. \quad (25)$$

This policy will need to fulfill two type of safety constraints. The first are state of charge constraints of the energy storage devices:

$$X_{safe,SOC} = \{x_{EMA} \in X_{EMA} \mid \begin{aligned} &SoC_{b,min} \leq SoC_b \leq SoC_{b,max} \\ &SoC_{FC,min} \leq SoC_{FC} \leq SoC_{FC,max} \end{aligned}\}, \quad (26)$$

where  $SoC_{b,min}, SoC_{FC,min}$  represent the minimum SoC levels for the energy storage devices, and  $SoC_{b,max}, SoC_{FC,max}$  their maximum values. The second set of constraints is the battery temperature

$$X_{safe,T} = \{x_{EMA} \in X_{EMA} \mid T_b \leq T_{b,max}\}. \quad (27)$$

This set of constraints can be temporarily violated; however, these violation increases the risk of failure of this component (e.g. thermal runaway [30]) and are penalized in the EMA performance score.

### C. Performance Metrics

The EMA will be evaluated using the following performance metrics (see also Table 2).

- $J_{E,tot}$ : Total energy: total energy consumption of the vehicle and the total energy losses. It is computed by integrating the power delivered by the battery ( $p_{bat}$ ), the fuel cell ( $p_{FC}$ ) and the power losses ( $p_{loss}$ ).
- $J_{SOC}$ : timespan that SoC constraints  $X_{safe,SOC}$  are violated.
- $J_{TC}$ : maximum temperature violation.
- $J_{deg}$ : battery capacity that is lost during the vehicle mission due to battery cycle aging.
- $J_v$ : derating metric that captures ability of the vehicle to track the velocity profile defined by the mission planning.
- $J_{tire}$ : Tire losses.

Table 2: Summary of performance metrics

| Metric      | Formula  |
|-------------|--|
| $J_{E,tot}$ | $\int_0^{t_{end}} (p_{bat}(t) + p_{FC}(t) + p_{loss}(t)) dt$ |
| $J_{SOC}$   | $\int \mathbb{1}_{\{x(t) \notin X_{safe,SOC}\}} dt$          |
| $J_{TC}$    | $\max_t \max(0, (T_{bat}(t) - T_{bat,max}))$                 |
| $J_{deg}$   | $\frac{d\Delta C_{cell}(i_{avg}, T_{avg})}{dN}$              |
| $J_v$       | $\int (1 - \alpha_v(t)) dt$                                  |
| $J_{tire}$  | $\int \left( \sum_i^4 p_{tire,i}(t) \right) dt$              |

$\mathbb{1}_{\{cond\}}$  is an indicator function that returns 1 if  $cond = 1$ , and zero otherwise

Note that the value of these performance metrics will be dependent on the EMA provided by the algorithm  $\pi(x)$  and the mission profile:

$$W = (v^*(t_k), \rho^*(t_k))_{k=1}^N. \quad (28)$$

### D. EMA Baseline Policy

The simulation model provided to the competitors contains a simple example policy, which is called baseline policy. This baseline policy is implemented as follows

$$\tilde{\pi}(x) = [\tilde{\alpha}_{FC}(x), \tilde{\alpha}_{AD}(x), \tilde{\alpha}_{TV}(x), \tilde{\alpha}_v(x)] \quad (29)$$

$$\tilde{\alpha}_{FC}(x) = \begin{cases} k_{FC} & \text{if } x(t) \in X_{safe,SOC} \\ 0 & \text{otherwise} \end{cases} \quad (30)$$

$$\tilde{\alpha}_{AD}(x) = 1/2 \quad (31)$$

$$\tilde{\alpha}_{TV}(x) = \frac{1}{2} + k_{TV}\rho^*(v^*)^2 \quad (32)$$

$$\tilde{\alpha}_v(x) = \begin{cases} 1 & \text{if } x(t) \in X_{safe,SOC} \\ \text{sat}(m_0 SoC_b + b_0), & \text{if } SoC_b(t) \leq SoC_{b,min} \\ \text{sat}(m_1 SoC_b + b_1), & \text{if } SoC_b(t) \geq SoC_{b,max} \end{cases} \quad (33)$$

This policy enforces

- constant usage of the fuel cell (with ratio  $k_{FC}$ ) if safety constraints are fulfilled (eq. (30)); it disables the fuel cell whenever violation of  $SoC$  constraints occur, eq. (33),
- constant front-rear torque distribution ratio, eq. (31),
- a torque allocation policy proportional to the expected lateral acceleration of the vehicle ( $\rho^*(v^*)^2$ ); where  $k_{TV}$  is a constant, eq. (32),
- a simple derating strategy that reduces the maximum vehicle velocity whenever the battery  $SoC$  are violated; see eq. (33) for details, where  $m_0, b_0, m_1, b_1$  are parameters and  $\text{sat}(\cdot)$  a saturation function that enforces the range  $[0,1]$ .

This baseline policy generates baseline metrics, which are denoted as  $\tilde{J}_{E,tot}, \tilde{J}_{SoC}, \tilde{J}_{TC}, \tilde{J}_{Deg}, \tilde{J}_v, \tilde{J}_{tire}$ .

Figure 7 shows an example of vehicle states and control inputs that were generated by the baseline EMA policy  $\tilde{\pi}(x)$  during an urban driving cycle.

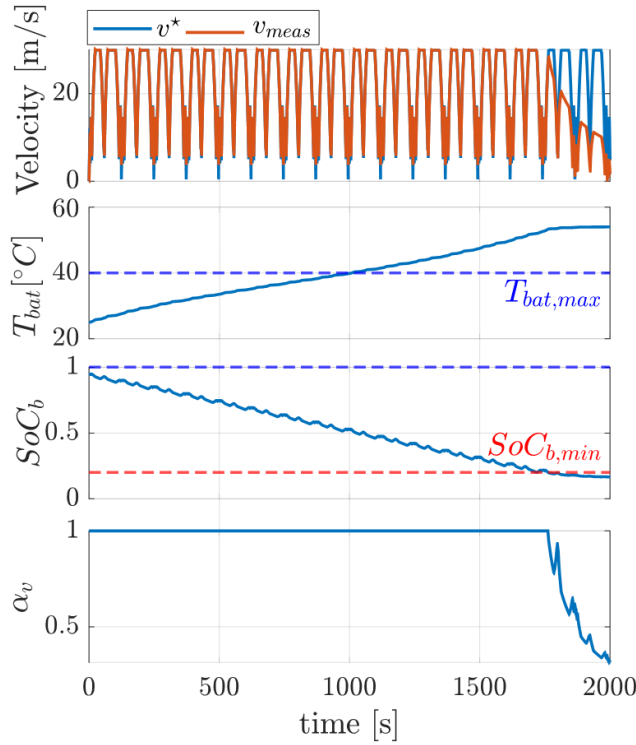


Figure 7: Example of a subset of vehicle states and control inputs generated by the vehicle model and EMA baseline policy

In this example, the battery temperature exceeds the upper limit at 1000 s, which might compromise battery safety. The derating strategy becomes active after 1800 s, decreasing  $\alpha_v$  and the maximum velocity (and maximum power) that the vehicle can reach.

Moreover, Figure 8 shows the histogram of the baseline performance metrics against 10 selected driving cycles. Some tracks are deliberately selected to be longer than what the car can fulfill to enforce maximum available energy consumption, velocity derating, and generating a baseline which could be improved upon smart design of EMAs' proposed by competitors.

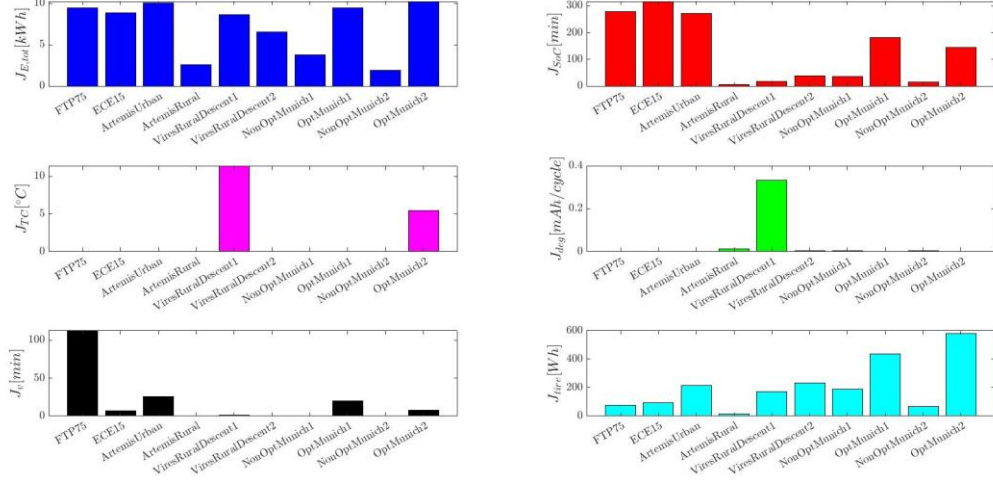


Figure 8: Performance metrics of the baseline policy against ten driving cycles.

The competitors are invited to develop better EMAs that can significantly avoid violation of the safety constraints, extend vehicle operation without loss of performance and reduced energy consumption.

### E. Evaluation and Ranking

The score of the EMA over a given mission profile is computed as a weighted summation of the performance metrics, normalized with respect to the EMA baseline policy ( $\tilde{\pi}$ ). Mathematically, this means:

$$J = k_{E,tot} \frac{J_{E,tot}}{\tilde{J}_{E,tot}} + k_{SoC} \frac{J_{SoC}}{\tilde{J}_{SoC}} + k_{TC} \frac{J_{TC}}{\tilde{J}_{TC}} + k_{Deg} \frac{J_{Deg}}{\tilde{J}_{Deg}} + k_v \frac{J_v}{\tilde{J}_v} + k_{tire} \frac{J_{tire}}{\tilde{J}_{tire}}, \quad (34)$$

where  $k_{E,tot}, k_{TC}, k_{Deg}, k_v, k_{tire}$  are known weights (defined by the organizers) and  $J_{E,tot}, J_{SoC}, J_{TC}, J_{Deg}, J_v, J_{tire}$  are the performance metrics obtained with the EMA provided by the competitor,  $\pi(x)$ . Please consider that if the baseline EMA performs well enough as any of the metrics  $\tilde{J}_x$  is resulted zero (e.g., it does not violate SoC constraints, or does not violate the maximum temperature limit), but the EMA designed by the competitor results in  $J_x \neq 0$ , then the overall performance metric will be penalized by a large number.

Moreover, note that the overall score of the EMA depends not only on the policy  $\pi(x)$ , but also on the mission profile  $W$ , i.e.,

$$J(\pi, W). \quad (35)$$

The evaluation will consider a bank of mission profiles  $W_1, W_2, \dots, W_M$ , which contain typical operating conditions for the vehicle. Each profile can be selected with probability

$$p(W_j) = p_j, \quad j = 1, \dots, M. \quad (36)$$

Some driving cycles (but not all) will be provided to the competitors; the driving cycle probability ( $p_j$ ) is also unknown to the competitors. The performance of an EMA will be performed based on the average cost over all mission profiles:

$$\mathbb{E}\{J(\pi, W)\} = \sum_{j=1}^M p(W_j) J(\pi, W_j), \quad (37)$$

where  $\mathbb{E}\{\cdot\}$  is the expected value operator (over  $W$ ). The final EMA ranking will be performed as follows. We will collect all the energy management algorithms provided by the competitors,  $\pi_1, \dots, \pi_L$ , where  $L$  is the number of received submissions. The competitor that provides the lowest average cost will be the winner, i.e.:

$$L_{winner} = \arg \min_{l \in \{1, \dots, L\}} \mathbb{E}\{J(\pi_l, W)\}. \quad (38)$$

## V. SUMMARY AND OUTLOOK

This article presents the conceptualization, modeling and setup for the IEEE Motor Vehicle Challenge 2023. It relies on a multi-domain modeling approach based on Modelica, FMI technology for a seamless model exchange between different

simulation tools, as well as an integrated vehicle control with trajectory following. Prospective competitors are invited to submit algorithms that can efficiently perform the energy management of the multiple electric motors and energy storage devices available in the reference vehicle. A wide range of performance metrics will be used to rank the submitted strategies, including energy consumption, fulfillment of safety constraints, battery degradation and loss of vehicle performance (derating).

The simulation framework will be available in the GitHub repository <https://github.com/DLR-VSDC/IEEE-MVC-2023> by November 2022. The repository will contain the vehicle model (FMU), the baseline energy management algorithm (MATLAB/Simulink) for an easy point-of-entry, and scripts to generate performance reports. The value of all vehicle and component parameters will be included in the repository to support the competitor's controller synthesis process.

Future points of interest in research are the development of more complex vehicle components and architectures which will be tuned and validated with real world experiments.

## VI. AUTHOR CONTRIBUTIONS

*Author Contributions:* Conceptualization, J.B., R.C., and J.T.; methodology, J.B., R.C., and J.T. Modelica vehicle model and components, J.B., and J.T.; controller and trajectories, R.C., and J.B.; EMA assessment and baseline algorithm: I.E., R.C. and J.B., library management and testing J.T., I.E., J.B.; writing—original draft preparation, R.C., J.B., J.T. and I.E.; All authors have read and agreed to the published version of the manuscript.

*Acknowledgement:* We would like to thank Basilio Lenzo for testing of challenge data and models.

*Funding:* internal institutional funding of the DLR granted by the Helmholtz Association of German Research Centres HGF.

## VII. REFERENCES

- [1] E. Amaya, H. Chiacchiarini, C. De Angelo und M. Asensio, „The Energy Management Strategy of FC/Battery Vehicles Winner of the 2017 IEEE VTS Motor Vehicles Challenge,“ in *The Energy Management Strategy of FC/Battery Vehicles Winner of the 2017 IEEE VTS Motor Vehicles Challenge*, 2017.
- [2] A. Ferrara und H. C., „Rule-Based Energy Management Strategy of Fuel Cell/Ultracapacitor/Battery Vehicles: winner of the IEEE VTS Motor Vehicles Challenge 2020,“ in *2020 IEEE Vehicle Power and Propulsion Conference*, 2020.
- [3] B. Nguyen; J. P. F. Trovão; S. Jemei; L. Boulon; A. Bouscayrol, „IEEE VTS Motor Vehicles Challenge 2021 - Energy Management of A Dual-Motor All-Wheel Drive Electric Vehicle,“ in *IEEE Vehicle Power and Propulsion Conference (VPPC)*, 2021.
- [4] C. Depature, S. Pagerit, L. Boulon, S. Jemei, A. Jemei und A. Bouscayrol, „IEEE VTS Motor Vehicles Challenge 2018 - Energy Management of a Range Extender Electric Vehicle,“ in *IEEE Vehicle Power and Propulsion Conference (VPPC)*, 2017.
- [5] H. Pereira, R. de Castro, R. E. Araújo, „How to Win the 2021 IEEE VTS Motor Vehicles Challenge With a Pragmatic Energy Management Strategy,“ in *IEEE Vehicle Power and Propulsion Conference (VPPC)*, 2021.
- [6] T. Vo-Duy, J. P. F. Trovão, S. Jemei, L. Boulon, M. C. Ta und A. Bouscayrol, „IEEE VTS Motor Vehicles Challenge 2022 - Sizing and Energy Management of Hybrid dual-Energy Storage System for a Commercial Electric Vehicle,“ in *2021 IEEE Vehicle Power and Propulsion Conference (VPPC)*, 2021.
- [7] J. Solano, S. Jemei, L. Boulon, L. Silva, D. Hissel, M-C Pera, „IEEE VTS motor vehicles challenge 2020-energy management of a fuel cell/ultracapacitor/lead-acid battery hybrid electric vehicle,“ in *IEEE Vehicle Power and Propulsion Conference (VPPC)*, 2019.
- [8] W. Lhomme; T. Letrouve; L. Boulon; S. Jemei; A. Bouscayrol; F. Chauvet; F. Tournez, „IEEE VTS Motor Vehicles Challenge 2019 - Energy Management of a Dual-Mode Locomotive,“ in *IEEE Vehicle Power and Propulsion Conference (VPPC)*, 2018.
- [9] R. de Castro, M. Tanelli, R. E. Araújo und S. M. Savaresi, „Design of safety-oriented control allocation strategies for overactuated electric vehicles,“ *Vehicle System Dynamics*, Vol. 52, pp. 1017-1046, 2014.
- [10] J. Torinsson, M. Jonasson, D. Yang und B. Jacobson, „Energy reduction by power loss minimisation through wheel torque allocation in electric vehicles: a simulation-based approach,“ *Vehicle System Dynamics*, Vol. 60, pp. 1488-1511, 2022.
- [11] B. Lenzo, „Torque Vectoring Control for Enhancing Vehicle Safety and Energy Efficiency,“ in *Vehicle Dynamics: Fundamentals and Ultimate Trends*, B. Lenzo, Pub., Cham, Springer International Publishing, 2022, p. 193–233.
- [12] C. Chatzikomis, A. Sorniotti, P. Gruber, M. Zanchetta, D. Willans und B. Balcombe, „Comparison of Path Tracking and Torque-Vectoring Controllers for Autonomous Electric Vehicles,“ *IEEE Transactions on Intelligent Vehicles*, Vol. 3, pp. 559-570, 2018.
- [13] R. de Castro und J. Brembeck, „Lyapunov-based fault tolerant control allocation,“ *Vehicle System Dynamics*, Vol. 0, pp. 1-26, 2021.
- [14] J. Brembeck, L. M. Ho, A. Schaub, C. Satzger, J. Tobolar, J. Bals und G. Hirzinger, „ROMO - The Robotic Electric Vehicle,“ in *22nd IAVSD International Symposium on Dynamics of Vehicle on Roads and Tracks*, Manchester Metropolitan University, 2011.
- [15] J. Brembeck und P. Ritzer, „Energy optimal control of an over actuated Robotic Electric Vehicle using enhanced control allocation approaches,“ in *Proceedings of the 2012 IEEE Intelligent Vehicles Symposium*, Alcalá de Henares, Spain, 2012.
- [16] J. Brembeck, „Model Based Energy Management and State Estimation for the Robotic Electric Vehicle ROboMObil,“ Ph.D. dissertation, Technical University of Munich, Munich, Germany, 2018.
- [17] DLR Vehicle System Dynamics Blog, „10 years ROboMObil,“ 08 2022. [Online]. Available: <https://vsdc.de/en/robomobil-timeline/>.
- [18] Modelica Association, „Modelica,“ 2022. [Online]. Available: <http://www.modelica.org>.

- [19] R. de Castro, T. Bünte und J. Brembeck, „Design and Validation of the Second Generation of the Robomobil's Vehicle Dynamics Controller,“ in *24th Symposium of the International Association for Vehicle System Dynamics*, Graz, Austria, 2016.
- [20] J. Ultsch, J. Mirwald, J. Brembeck und R. de Castro, „Reinforcement Learning-based Path Following Control for a Vehicle with Variable Delay in the Drivetrain,“ in *31st IEEE Intelligent Vehicles Symposium*, 2020.
- [21] T. Bünte, L. M. Ho, C. Satzger und J. Brembeck, „Central Vehicle Dynamics Control of the Robotic Research Platform ROboMObil,“ *ATZechnik worldwide*, June 2014.
- [22] D. Zimmer, „A Planar Mechanical Library for Teaching Modelica,“ in *Proceedings of the 9th International Modelica Conference*, Munich, Germany, 2012.
- [23] D. Zimmer und M. Otter, „Real-time models for wheels and tyres in an object-oriented modelling,“ *Vehicle System Dynamics*, 2009.
- [24] J. Brembeck, „A Physical Model-Based Observer Framework for Nonlinear Constrained State Estimation Applied to Battery State Estimation,“ *Sensors*, Vol. 19, Nr. 20, p. 4402, 2019.
- [25] R. de Castro, H. Pereira, R. E. Araújo, J. V. Barreras und H. C. Pangborn, „qTSL: A Multilayer Control Framework for Managing Capacity, Temperature, Stress, and Losses in Hybrid Balancing Systems,“ *IEEE Transactions on Control Systems Technology*, Vol. 30, pp. 1228-1243, 2022.
- [26] Wikipedia, „Modelica,“ 08 2022. [Online]. Available: <https://en.wikipedia.org/wiki/Modelica>.
- [27] D. Feroldi, M. Serra und J. Riera, „Energy Management Strategies based on efficiency map for Fuel Cell Hybrid Vehicles,“ *Journal of Power Sources*, Vol. 190, pp. 387-401, 2009.
- [28] K. J. Åström und R. M. Murray, *Feedback Systems: An Introduction for Scientists and Engineers*, Second Edition, Princeton University Press, 2021.
- [29] J. Ackermann, P. Blue, T. Bünte, L. Guvenc, D. Kaesbauer, M. Kordt, M. Muhler und D. Odenthal, *Robust Control: The Parameter Space Approach*, 2002.
- [30] X. Feng, D. Ren, X. He und M. Ouyang, „Mitigating Thermal Runaway of Lithium-Ion Batteries,“ *Joule*, Vol. 4, pp. 743-770, 2020.